Nanoscale

Accepted Manuscript

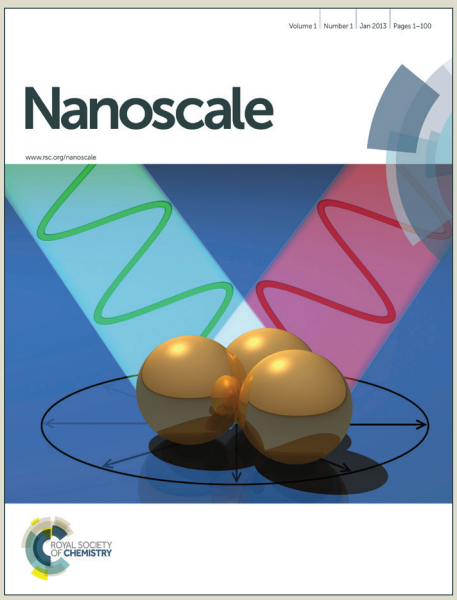

ROYAL SOCIETY OF CHEMISTRY

www.rsc.org/nanoscale

A new route toward light emission from Ge: tensile-strained quantum dot

Qimiao Chen,[ab] Yuxin Song,*[a] Kai Wang,[a] Li Yue,[a] Pengfei Lu[c], Yaoyao Li,[a] Qian Gong,[a] and Shumin Wang*[ad]

Abstract: Tensile-strained Ge quantum dot (QD) is proposed as a new route for the realization of direct bandgap conversion in Ge. Ge QDs were successfully grown on InP substrate by molecular beam epitaxy. The strain field in the QDs were analyzed by high resolution transmission electron microscopy and simulated by finite element method based on the measured geometries. The strain field in the QDs is found non-uniform and the shear component plays a significant role on the energy band structure leading to larger required hydrostatic strain than that in the Ge thin films under biaxial strain to become a direct bandgap.

Germanium (Ge) is one of the earliest studied semiconductors and offers a wide range of important electronic and optoelectronic device applications. The compatibility with current Si based integrated circuits would be the most important feature for Ge to be a promising candidate material for future high speed electronics and Si photonics. In microelectronics, due to the high mobility of both electrons and holes and compatibility with complementary metal-oxide-semiconductor (CMOS) processing, Ge has been made for high speed CMOS-based devices.[1, 2] In optoelectronics, Ge is a promising material for photodetector,[3] light emitters[4, 5] and solar cells.[6] More interestingly, it has been theoretically predicted that 1.4% biaxial tensile strain can fill up the 136 meV gap between the Γ and L valley,[7] thereby converting Ge into a direct-bandgap semiconductor with a corresponding wavelength around 1.55 μm, making the tensile-strained Ge one of the most promising candidates to construct light sources for Si-photonics integration. Furthermore, the tensile strain modifies the curvature of the energy bands near their extrema, and thus increases the carrier mobility dramatically,[7, 8] especially for the hole, leading to potential high speed CMOS.

To prove and utilize the fascinating properties, different approaches have been proposed to introduce tensile strain into Ge. The difference in thermal dilation coefficients between Ge and Si allows one to introduce 0.25% tensile strain in Ge thin films after the Ge film is cooled down from the growth temperature.[9] Growth of Ge on templates with a lattice constant larger than that of Ge, like InGaAs[8, 10-12] or GeSn,[13] can introduce high biaxial tensile strain. Another approach is based on the use of micromechanical strain engineering or an external stressor.[14-19] Up to date, the large lattice constant buffer method has made the most significant progresses. As large as 2.33% tensile strain has been achieved in a Ge thin film on a relaxed InGaAs buffer layer and signature of a direct band-gap emission was indicated from low-temperature photoluminescence.[11] However, there are many challenges difficult to overcome for this method. Firstly, with such a large tensile strain to convert the bandgap, the critical thickness for plastic relaxation is only a few nanometers. Some technical problems need to be solved as well. The relaxed buffer layers almost unavoidably possess rough surface and a high density of threading dislocations coming from the underneath templates, both of which are harmful for the structural and optical quality of the Ge films.

Here we propose a new route, tensile-strained quantum dot (QD), to realize direct bandgap conversion in Ge. Compared with thin film, QDs can hold large strain without plastic relaxation and are much less sensitive to defects such as roughness and dislocations. They have already been widely utilized in different kinds of optoelectronic devices with high temperature stability of the threshold current density[20, 21] and giant material gain[22, 23] etc. Other technical advantages include suppression of diffusion of non-equilibrium carriers, which leads to reduced leakage of non-equilibrium carriers from the ridge region, suppression of non-radiative recombination at point and extended defects and blocking of dislocation propagation.[24] Therefore, the combination of tensile strain with QD will be a promising scheme to realize direct band-gap gain material and subsequently Ge based light emitters. However, there are some issues to be considered. Firstly, the tensile strain will be partially relaxed through elastic deformation during the formation of QDs and therefore it is a question of whether the residual strain is still large enough to hold the direct bandgap. Secondly, the spatial distribution of residual strain inside a QD is non-uniform and how this will affect the electronic structures in a QD is unclear. Thirdly, the shear strain component which is negligible in thin films is nonzero in QDs and its effect on energy band can't be neglected.

In this work, we consider Ge QDs on InP as a prototype model with a lattice mismatch as large as 3.7% and grow such Ge QDs by molecular beam epitaxy (MBE).Surface morphology is assessed by atomic force microscope (AFM) and the strain field distribution inside Ge QDs is investigated by high resolution cross-sectional transmission electron microscopy (TEM). We employ the finite element method (FEM) to simulate strain field distribution inside Ge QDs with size and morphology measured by TEM. Deformation potential theory[25] is applied to calculate strain field induced change of band edges at the relevant valleys taking into account the effect of shear strain. We show that direct-bandgap region is indeed maintained in the QDs when the width to height (W/H) ratio of the QD is sufficiently large, indicating the great potential of tensile-strained Ge QDs for optoelectronic applications.

Tensile-strained Ge QDs were grown on *n*-type (100) InP substrates by MBE. Prior to the growth, the surface oxide desorption of the InP substrate was carried out at about 500 ˚C. After that, a 150 nm thick InP buffer layer was grown at 450 ˚C to improve surface quality. Finally a Ge QD layer was grown with an equivalent thin film thickness of 0.95 nm at a rate of 190 nm/h at 450 ˚C. Formation of QD was confirmed by reflection high-energy electron diffraction (RHEED) in situ and by AFM *ex situ* with a typical example shown in Fig. 1(a). 40 randomly chosen QDs were investigated for statistics. TEM measurements were carried out and the strain field was computed by geometric phase analysis (GPA).[26] The strain field of the same Ge QD was simulated by FEM. It is observed from the TEM images that the

Ge QDs are epitaxially grown on InP confirming a diamond crystal structure of the Ge QDs. The FEM simulations in this work all based on zinc-blend-structure InP and diamond-structure Ge. The initial tensile strain before relaxation is

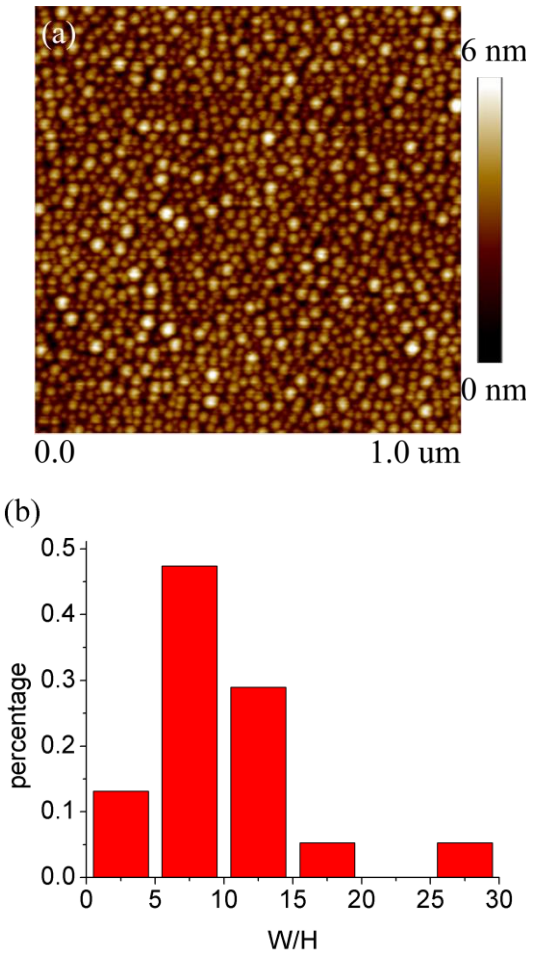

Figure 1 (a) AFM image of the tensile-strained Ge QDs on InP. (b) Statistical distribution of QDs as a function of measured W/H ratio

3.7% induced by the lattice mismatch between Ge and InP. The strain effect on bandgap shift of the Ge is discussed by the deformation potential theory. The elastic constants of Ge[27] and InP[28] used in the simulations are from references.

From the morphology of the Ge QDs obtained from AFM, the lateral sizes of the QDs are larger than the electron coherence length and can be treated as a quasi-2D system. The effect of strain on energy bandgaps can be explained by the deformation potential theory. Ge is an indirect-bandgap material whose conduction band minima is at the *L*-valley. To convert Ge into a direct-bandgap material, tensile strain must be applied to reduce the difference between the *L*-valley and the *Γ*-valley. The direct conduction band of the *Γ*-valley is only subject to hydrostatic strain as following:

$$\Delta E_c^{\Gamma} = a_c * (\varepsilon_{xx} + \varepsilon_{yy} + \varepsilon_{zz}) \quad (1)$$

Where a_c is hydrostatic deformation potential at the *Γ* point,[29] ε_{xx}, ε_{yy} and ε_{zz} are strain in x direction, stain in y direction and strain in z direction, respectively. Here we assume that x direction, y direction and z direction are [1 0 0] direction, and [0 1 0] direction and [0 0 1] direction, respectively. Because of the cubic symmetry, the conduction band valley at the *L* point is degenerate and the shear strain component leads to a split of the *L*-valley by reducing the symmetry.

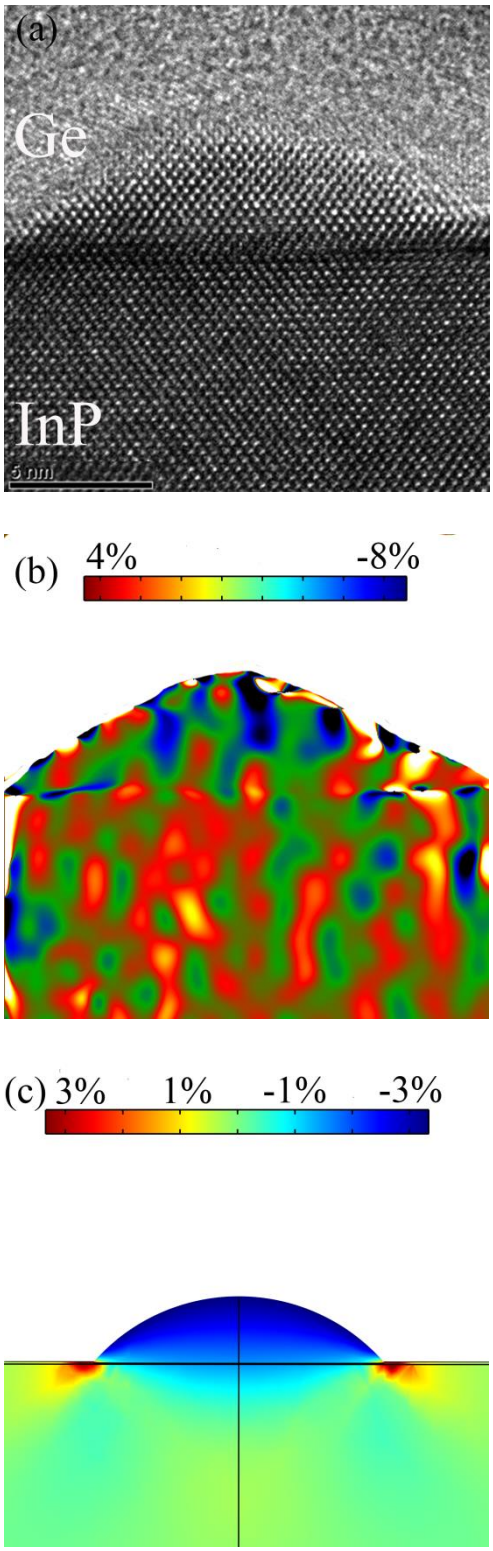

Fig. 2 HRTEM image of a QD with a bottom width of 15 nm and a height of 3.4 nm, (b) in-plane strain field distribution by GPA of the same Ge QD and (c) in-plane strain field simulated by FEM

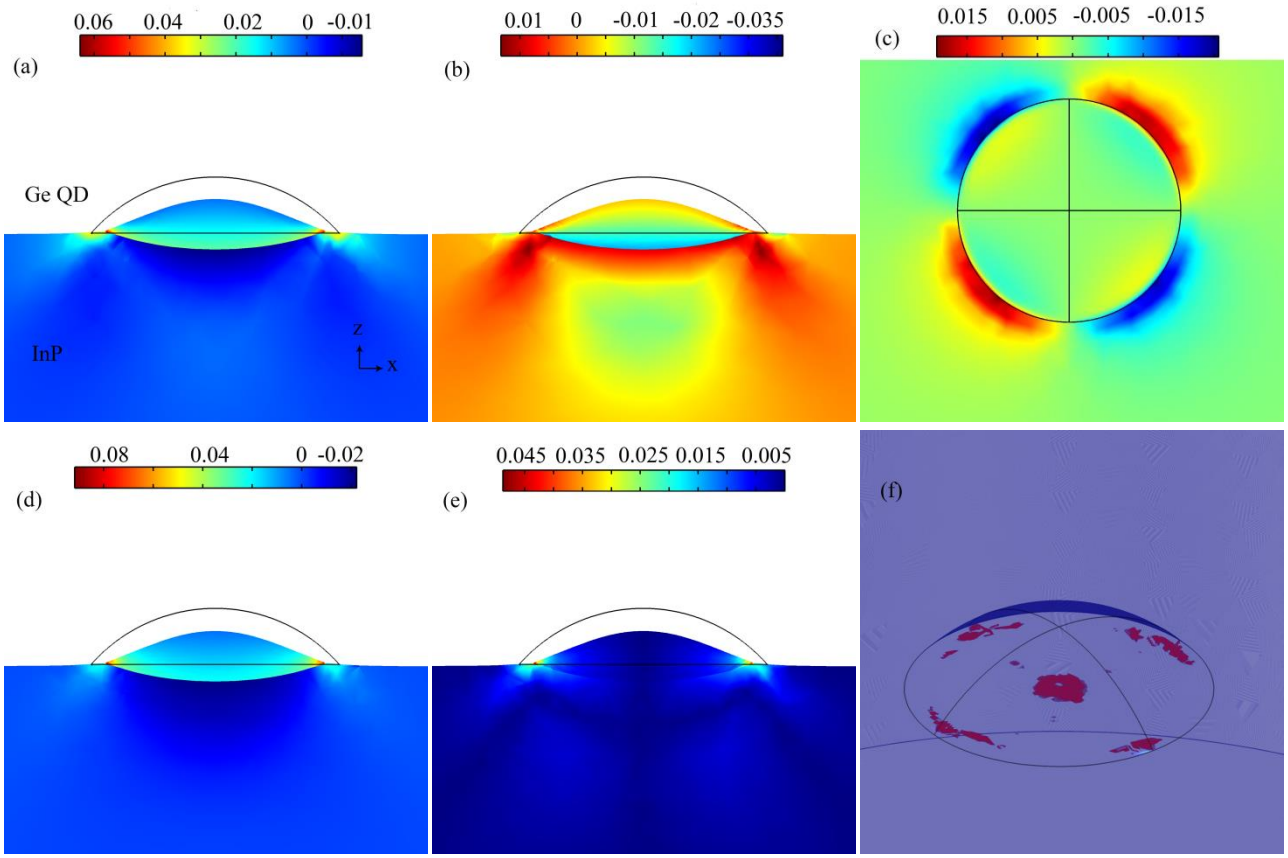

Fig. 3 The FEM simulation results of the strain components in the xz cross section: (a) the parallel strain ε_{xx}, (b) the vertical strain ε_{zz}, (c) the shear strain ε_{xy}, (d) the hydrostatic strain, and (e) the sum of absolute value of shear strain components. (f) the converted direct bandgap part in the Ge QD marked with red. The deformation is 10 times exaggerated.

of valley i under a homogeneous deformation described by the strain tensor $\overleftrightarrow{\varepsilon}$ can be expressed as

$$\Delta E_c^i = \left(\Xi_d \overleftrightarrow{1} + \Xi_u \{\boldsymbol{a}_i \boldsymbol{a}_i\}\right) : \overleftrightarrow{\varepsilon} \quad (2)$$

Where $\overleftrightarrow{1}$ is the unit tensor, $\boldsymbol{a}_i$ is the unit vector parallel to the $\boldsymbol{k}$ vector of valley i, Ξ_d and Ξ_u are dilation deformation potential and uniaxial deformation respectively. { } denotes a dyadic production. The values for the deformation potentials Ξ_d and Ξ_u at *L*-valley of Ge are -6.97 eV and 16.3 eV, respectively. For diamond structure, there are eight equivalent *L*-valleys. To convert Ge into a direct bandgap material, the *Γ*-valley should be lower than all the split *L*-valleys. The energy shift of the lowest *L*-valley is

$$\Delta E_c^L = \left(\Xi_d + \frac{1}{3}\Xi_u\right) * Tr\overleftrightarrow{\epsilon} - \frac{2}{3}\Xi_u * (|\varepsilon_{xy}| + |\varepsilon_{xz}| + |\varepsilon_{yz}|) \quad (3)$$

Thus when

$$\Delta E_c^\Gamma - \Delta E_c^L < -136\ meV \quad (4)$$

where 136 meV is the energy difference between the *L*-valley and the *Γ*-valley of unstrained Ge, the tensile strained Ge becomes a direct bandgap semiconductor.

Following the notation of Herring and Vogt,[25] the energy shift

Figure 1(a) shows an AFM image of Ge QDs grown on InP while the statistical size distribution of the QDs as a function of the W/H ratio is shown in Fig. 1(b). The W/H ratio considering the AFM tip effect is found varied from 5 to 30 with a peak around 10. The width of the QDs ranges from 4 nm to 32nm and the height ranges from 0.7 nm to 3.5 nm.

A high-resolution TEM (HRTEM) image of a QD is shown in Fig. 2(a). As seen, the QD has a spherical cap shape with a bottom width of 15nm and a height of 3.4 nm, and is free of defects. The 2-dimensional map of the parallel strain ε_{xx} obtained from the analysis of the HRTEM by GPA is shown in Fig. 2(b). The InP buffer in the image is taken as the reference lattice for the calculations and the strain here is defined as $(a_{Ge} - a_{InP})/a_{InP}$, where a_{Ge} and a_{InP} are the lattice constant of Ge and of InP, respectively. The precision of GPA highly depends on the quality of HRTEM images. The lower InP part in Fig.2 (a) is taken as the reference region and the error range of strain in GPA based on our best TEM images is estimated to be around 2%. Limited by the quality of the HRTEM image and the resolution of

the GPA method, the analysis can only be implemented comparatively. In Fig. 2(b), the top QD region shows negative strain in average indicating large strain relaxation. The strain field at the bottom region of the QD is similar to that of the InP showing that the lattice is strained and the strain at the peripherals is extremely large. The simulation also supports the GPA results as shown in Fig. 2(c). The simulated strain is relaxed gradually from the QD/buffer interface toward surface within the QD and the maximum strain is at the peripherals. The strain obtained from HRTEM images could be affected by the relaxation occurred during the preparation of the TEM samples.

The strain field in the same QD shown in Fig. 2(a) is simulated by FEM based on a 3D spherical cap model with a width of 15

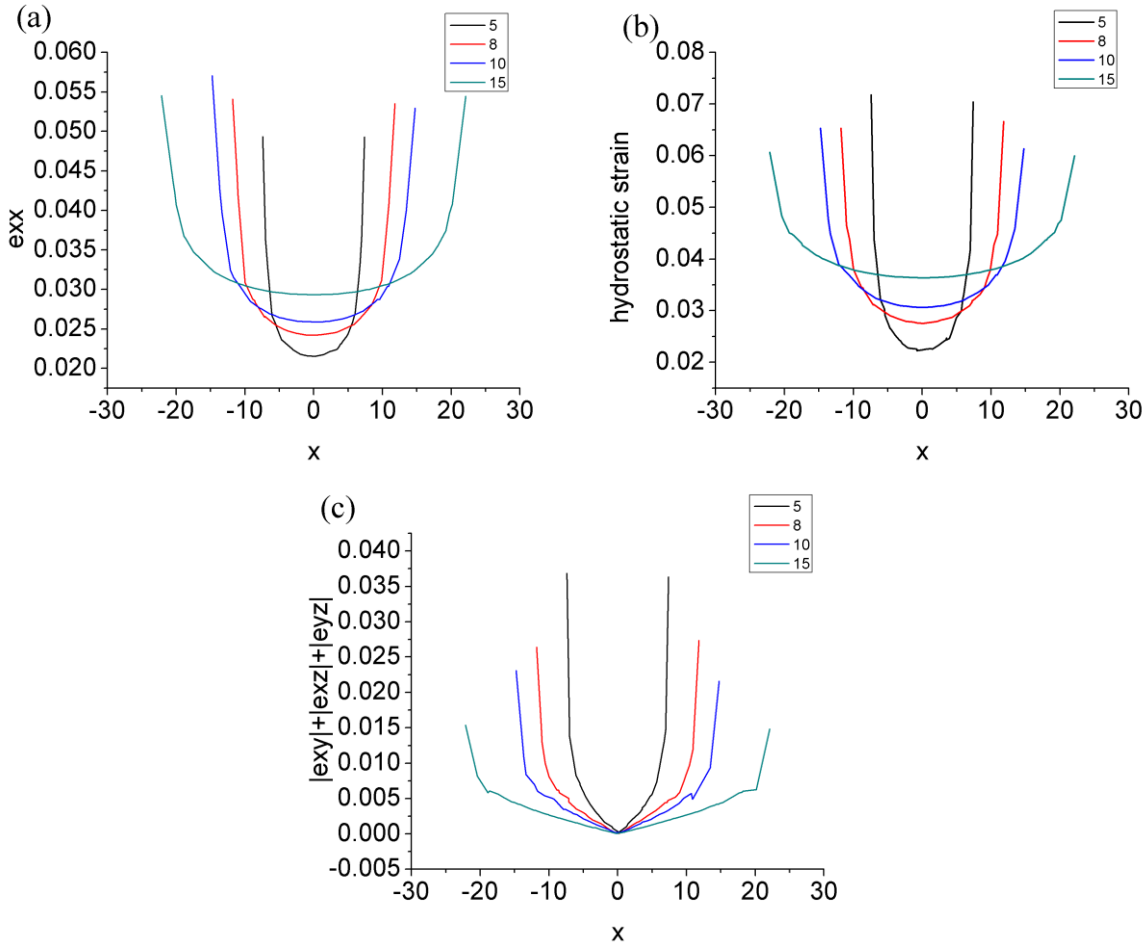

Fig. 4 strain along line A and the volume percentage of the direct bandgap in the QD with different W/H. (a) ε_{xx} (b) hydrostatic strain (c) $|\varepsilon_{xy}| + |\varepsilon_{xz}| + |\varepsilon_{yz}|$

nm and a height of 3.4 nm. We define the strain as $(a_{Ges} - a_{Ge})/a_{Ge}$, where a_{Ges} and a_{Ge} are the lattice constants of the strained Ge and the relaxed Ge, respectively. The strain components of the xz cross section are shown in Fig. 3. Figure 3(a) shows that in the direction perpendicular to the QD/InP interface, ε_{xx} decreases from the bottom to the top of the QD with a maximum value 6.5% at the peripherals, which is even larger than the lattice mismatch of 3.7% between Ge and InP. Also the upper part of InP is deformed influenced by the deposited Ge QD. Meanwhile, the strain in top of the QD is almost fully relaxed. The volume average of ε_{xx} in the QD is 1.5%. The vertical strain field, ε_{zz} in the z direction decreases with increasing height within the QD as shown in Fig. 3(b). Different from biaxial strain in thin films, the shear strain component in the QDs has a strong effect on the energy band structure and can't be neglected, as seen in Fig. 3(c). The shear strain is large at peripherals and not symmetrical. According to equation (1) and (3), the bandgap conversion depends on both the hydrostatic strain and the sum of the absolute values of the three shear strain components. Hydrostatic strain has similar characteristics with ε_{xx} as shown in Fig. 3(d). The sum of the absolute values of the shear components decreases from the peripherals to the center and is comparable to hydrostatic strain as shown in Fig. 3(e). Considering both the hydrostatic strain and the shear strain components, the direct bandgap part of the QD is calculated and shown in Fig. 3(f) in red. As seen, the strain effect in QDs is different from the biaxial strain effect in bulk or thin films. The hydrostatic strain in the bottom of the QD is larger than the critical hydrostatic strain which is needed to convert Ge thin films into direct bandgap. But it is not large enough to

convert the QD into direct bandgap due to the effect of the shear strain components which do not exist in biaxial strained Ge thin films. Comparing the deformation potential Ξ_u with $(\Xi_d + \Xi_u/3)$, we discover that the effect of shear strain on the bandgap shift is 7 times as strong as for the effect caused by hydrostatic strain.

To find out the effect of QD geometry on strain and energy band, Ge QD with different W/H ratios (H is kept at 3 nm) is (1) and equation (3), hydrostatic strain decides the width of bandgap at Γ point, and thus the direct bandgap of the QDs decreases with the increasing W/H as shown in Fig. 4(b). As shown in Fig. 4(c), the sum of the absolute values of the three shear strain components in the center is zero, and thus the center part is more easily to be converted into direct bandgap. The increased sum of the absolute values of the three shear strain components apart the center suppresses the bandgap conversion. Besides, shear strain decreases with the increasing W/H. Considering the effect of hydrostatic strain and shear strain on energy band, Ge QD with larger W/H is easier to be converted into direct bandgap.

Almost no photoluminescence was observed from the tensile-strained Ge QD sample. The reason can be that Ge/InP heterostructure has a type-II band alignment resulting in confinement only for the holes but barrier for the electrons. According to the model-solid theory, the unstrained Ge and InP form a type-II band alignment, leading to only confinements for the holes with a band offset of 0.75 eV but a barrier to the electrons with a band offset of 0.22 eV. Although tensile strain will reduce the barrier, the confinements for electrons will still be weak due to the large QCEs which will elevate the energy levels in the Ge QDs. Inter-diffusion is another factor should be considered in a system with such large strain. Energy-dispersive X-ray spectroscopy (EDS) mapping (not shown here) weakly hints that In atoms seem to have diffused into the Ge QDs, limited by the spatial resolution. The In atoms in the QDs may act as non-radiative recombination centers. Some other factors, e.g. quantum confinement effect (QCE) and surface states may also affect the band structures and the optical properties in the tensile-stained Ge QDs. The QCE will elevate the energy levels in the QDs and would promote the electron tunnelling between the valleys, leading to extra difficulty for a direct bandgap conversion and radiative recombination. The effects from the surface states is not clear yet and will be investigated in the future work. For the future experiments, a type-I band structure, e.g. $In_{0.52}Al_{0.48}As$/Ge QD/ $In_{0.52}Al_{0.48}As$ or $AlAs_{0.56}Sb_{0.44}$/Ge QD/ $AlAs_{0.56}Sb_{0.44}$, should be designed to study the optical properties of the tensile-strained Ge QDs.

In conclusion, Tensile-strained Ge QDs were successfully grown on InP by MBE and the strain field of the QDs were analyzed both theoretically and experimentally. The strain field in the QDs is found non-uniform and the shear component plays an significant role on the energy band structure in a way that the degenerated *L*-valleys splits as a result of the reduced crystal symmetry, thus increasing the difficulty of reaching the direct bandgap. The residual strain increases with the increasing W/H ratio of the QDs. This work shows that tensile-strained Ge QDs can be a promising route toward light emission from Ge for future optoelectronic applications, such as lasers on Si.

simulated. ε_{xx}, hydrostatic strain and the sum of absolute values of three shear strain components along line A are shown in Fig. 4(a)-(c), respectively. As seen in Fig. 4(a), the minimum of ε_{xx} is in the center while the maximum is at the edges. The minimum increases with the increasing W/H indicating that the QD with larger W/H holds more residual strain. The hydrostatic strain in Fig. 4(b) shows the similar characteristics. According to equation

ACKNOWLEDGMENT

The authors would like to thank the financial support from the Natural Science Foundation of China (Grant No. 61404153), the Shanghai Pujiang Program (Grant No.14PJ1410600), the Key Program of Natural Science Foundation of China (Grant No. 61334004), the National Basic Research Program of China (973) (Grant No. 2014CB643902), Strategic Priority Research Program of the Chinese Academy of Sciences (Grant No. XDA5-1), the Key Research Program of the Chinese Academy of Sciences (Grant No. KGZD-EW-804), the Creative Research Group Project of Natural Science Foundation of China (Grant No. 61321492), the International Collaboration and Innovation Program on High Mobility Materials Engineering of Chinese Academy of Sciences and the Open Program of State Key Laboratory of Functional Materials for Informatics.

Notes and references

[a] *State Key Laboratory of Functional Materials for Informatics, Shanghai Institute of Microsystem and Information Technology, CAS, Shanghai, China. E-mail: songyuxin@mail.sim.ac.cn*
[b] *University of Chinese Academy of Sciences, Beijing*
[c] *State Key Laboratory of Information Photonics and Optical Communications, Ministry of Education, Beijing University of Posts and Telecommunications, P.O. Box 72, Beijing. E-mail: photon@bupt.edu.cn*
[d] *Department of Microtechnology and Nanoscience, Chalmers University of Technology, Gothenburg, Sweden. E-mail: shumin@mail.sim.ac.cn*

1. K. Saraswat, C. O. Chui, T. Krishnamohan, D. Kim, A. Nayfeh and A. Pethe, *Materials Science and Engineering B-Solid State Materials for Advanced Technology*, 2006, **135**, 242-249.
2. S. C. Jain, S. Decoutere, M. Willander and H. E. Maes, *Semiconductor Science and Technology*, 2001, **16**, R67-R85.
3. J. Michel, J. Liu and L. C. Kimerling, *Nat Photon*, 2010, **4**, 527-534.
4. P. Boucaud, M. El Kurdi, A. Ghrib, M. Prost, M. de Kersauson, S. Sauvage, F. Aniel, X. Checoury, G. Beaudoin, L. Largeau, I. Sagnes, G. Ndong, M. Chaigneau and R. Ossikovski, *Photon. Res.*, 2013, **1**, 102-109.

5. J. F. Liu, X. C. Sun, R. Camacho-Aguilera, L. C. Kimerling and J. Michel, *Optics Letters*, 2010, **35**, 679-681.
6. N. E. Posthuma, J. van der Heide, G. Flamand and J. Poortmans, *Electron Devices, IEEE Transactions on*, 2007, **54**, 1210-1215.
7. M. V. Fischetti and S. E. Laux, *Journal of Applied Physics*, 1996, **80**, 2234.
8. Y. Bai, K. E. Lee, C. Cheng, M. L. Lee and E. A. Fitzgerald, *Journal of Applied Physics*, 2008, **104**.
9. Y. Ishikawa, K. Wada, D. D. Cannon, J. Liu, H.-C. Luan and L. C. Kimerling, *Applied Physics Letters*, 2003, **82**, 2044.
10. R. Jakomin, M. de Kersauson, M. El Kurdi, L. Largeau, O. Mauguin, G. Beaudoin, S. Sauvage, R. Ossikovski, G. Ndong, M. Chaigneau, I. Sagnes and P. Boucaud, *Applied Physics Letters*, 2011, **98**.
11. Y. Huo, H. Lin, R. Chen, M. Makarova, Y. Rong, M. Li, T. I. Kamins, J. Vuckovic and J. S. Harris, *Applied Physics Letters*, 2011, **98**, 011111.
12. M. de Kersauson, M. Prost, A. Ghrib, M. El Kurdi, S. Sauvage, G. Beaudoin, L. Largeau, O. Mauguin, R. Jakomin, I. Sagnes, G. Ndong, M. Chaigneau, R. Ossikovski and P. Boucaud, *Journal of Applied Physics*, 2013, **113**.
13. Y. Y. Fang, J. Tolle, R. Roucka, A. V. G. Chizmeshya, J. Kouvetakis, V. R. D'Costa and J. Menendez, *Applied Physics Letters*, 2007, **90**.
14. D. Nam, D. Sukhdeo, S. L. Cheng, A. Roy, K. C. Y. Huang, M. Brongersma, Y. Nishi and K. Saraswat, *Applied Physics Letters*, 2012, **100**.
15. D. Nam, D. Sukhdeo, A. Roy, K. Balram, S. L. Cheng, K. C. Y. Huang, Z. Yuan, M. Brongersma, Y. Nishi, D. Miller and K. Saraswat, *Optics Express*, 2011, **19**, 25866-25872.
16. C. Boztug, J. R. Sanchez-Perez, F. F. Sudradjat, R. B. Jacobson, D. M. Paskiewicz, M. G. Lagally and R. Paiella, *Small*, 2013, **9**, 622-630.
17. J. R. Sanchez-Perez, C. Boztug, F. Chen, F. F. Sudradjat, D. M. Paskiewicz, R. B. Jacobson, M. G. Lagally and R. Paiella, *Proceedings of the National Academy of Sciences of the United States of America*, 2011, **108**, 18893-18898.
18. P. H. Lim, S. Park, Y. Ishikawa and K. Wada, *Optics Express*, 2009, **17**, 16358-16365.
19. M. El Kurdi, H. Bertin, E. Martincic, M. de Kersauson, G. Fishman, S. Sauvage, A. Bosseboeuf and P. Boucaud, *Applied Physics Letters*, 2010, **96**.
20. N. Kirstaedter, N. N. Ledentsov, M. Grundmann, D. Bimberg, V. M. Ustinov, S. S. Ruvimov, M. V. Maximov, P. S. Kopev, Z. I. Alferov, U. Richter, P. Werner, U. Gosele and J. Heydenreich, *Electronics Letters*, 1994, **30**, 1416-1417.
21. M. Asada, Y. Miyamoto and Y. Suematsu, *Ieee Journal of Quantum Electronics*, 1986, **22**, 1915-1921.
22. D. Bimberg, N. Kirstaedter, N. N. Ledentsov, Z. I. Alferov, P. S. Kopev and V. M. Ustinov, *Ieee Journal of Selected Topics in Quantum Electronics*, 1997, **3**, 196-205.
23. N. Kirstaedter, O. G. Schmidt, N. N. Ledentsov, D. Bimberg, V. M. Ustinov, A. Y. Egorov, A. E. Zhukov, M. V. Maximov, P. S. Kopev and Z. I. Alferov, *Applied Physics Letters*, 1996, **69**, 1226-1228.
24. Z. Mi, J. Yang, P. Bhattacharya and D. L. Huffaker, *Electronics Letters*, 2006, **42**, 121-123.
25. C. Herring and E. Vogt, *Physical Review*, 1956, **101**, 944-961.
26. M. J. Hÿtch, E. Snoeck and R. Kilaas, *Ultramicroscopy*, 1998, **74**, 131-146.
27. S. P. Nikanorov and B. K. Kardashev, *Elasticity and Dislocation Inelasicity of Crystalls*, Nauka Publ. House, Russian, 1985.

28. D. N. Nichols, D. S. Rimai and R. J. Sladek, *Solid State Communications*, 1980, **36**, 667-669.

29. C. G. Van De Walle, *Physical Review B*, 1989, **39**, 1871-1883.